Transgenic porcine model reveals two roles for LGR5 during lung development and homeostasis

Kathryn M. Polkoff[1,2], Nithin K. Gupta[2,3], Yanet Murphy[1,2], Ross Lampe[1,2], Jaewook Chung[1,2], Amber Carter[1,2], Jeremy M. Simon[4], Katherine Gleason[1,2], Adele Moatti[2,5], Preetish K. Murthy[6], Laura Edwards[1,2], Alon Greenbaum[2,5], Aleksandra Tata[6], Purushothama Rao Tata[6], Jorge A. Piedrahita*[1,2]

Author Affiliation:

Department of Molecular Biomedical Sciences, College of Veterinary Medicine, North Carolina State University, Raleigh, NC 27607, USA

Comparative Medicine Institute, North Carolina State University, Raleigh, NC 27607, USA

Campbell University School of Osteopathic Medicine, Lillington, NC 27546, USA

Department of Genetics, University of North Carolina School of Medicine

Joint Department of Biomedical Engineering, University of North Carolina at Chapel Hill and North Carolina State University, Raleigh/Chapel Hill, NC 27607/27599, USA

Department of Cell Biology, Duke University School of Medicine, Durham, NC, USA

*Corresponding Author Jorge A. Piedrahita
Department of Molecular Biomedical Sciences and Comparative Medicine Institute
North Carolina State University japiedra@ncsu.edu

ABSTRACT
Stem cells play a pivotal role in lung homeostasis, repair, and regeneration, and yet the mechanisms underlying these processes are unknown. Furthermore, species-specific differences make certain findings from mice, a widely used animal model, difficult to translate into humans. In this work, we address these limitations by using a transgenic pig model and identify two populations of LGR5+ cells in the lung. Interestingly, we found similar populations in human lungs but not in mice. Using RNA sequencing, 3D imaging, organoid models, and differentiation assays, we determine that in the fetal lung, epithelial LGR5 expression is transient in a subpopulation of developing lung bud tips, co-expresses bud tip markers SOX9 and SFTPC. While epithelial LGR5 expression is absent from postnatal lung, it is reactivated in bronchioalveolar organoids derived from basal airway cells. A separate population of LGR5+ cells is mesenchymal, surrounds developing and mature airways, lies adjacent to airway basal cells, is closely associated with nerve fibers, and acts as a multipotent progenitor cell capable of supporting the airway basal cell niche. Transcriptionally, mesenchymal LGR5+ cells are analogous to stromal stem cell populations and express unique patterns of WNT and TGFbeta signaling pathway genes. These results point to two roles for LGR5 in orchestrating stem and progenitor cell dynamics and provide a physiologically relevant model for further studies on the role of these populations in repair and regeneration.

Introduction

LGR5, a surface receptor for R-spondin, is a known potentiator of WNT signaling (1). LGR5 is often involved in developmental processes and regeneration, and generally marks key progenitor populations in organ development or postnatal homeostasis. Originally identified in the intestine (2), LGR5$^+$ populations have been identified in an increasing number of tissues and organs (3). Until the advent of scRNAseq, one organ that has been largely unstudied regarding the role of LGR5 was the lung. WNT signaling has long been known to be vital to lung development (4, 5) in addition to repair and regeneration (6). Furthermore, RSPO2, the ligand for LGR5, was shown to have a vital role in lung branching morphogenesis, and the limited lung growth resulting from inactivation of RSPO2 was correlated with reduced canonical WNT signaling (7). Both pathways suggest a potential role for LGR5 signaling, but in the developing lung, Lgr5$^+$ cells have not been described in mice. However, using scRNAseq, an *LGR5*$^+$ epithelial population was recently reported in the elongating bud tip of the human fetal lung (8).

In the postnatal lung, a study of Lgr5 expression in mice describes a unique role for Lgr5$^+$ mesenchymal cells which are absent from the airways but centered around the alveolar progenitor cells orchestrating the alveolar niche (9). More recently, however, using scRNA analysis of the human lung, *LGR5*$^+$ mesenchymal cells were identified as airway-associated cells (10).

The disconnect between the human and murine cell population calls for an animal model that represents a more faithful anatomical and physiological model to the human lung (11–14). Here we used a transgenic porcine model expressing a nuclear-localized histone H2B–GFP under the control of the endogenous *LGR5* promoter (15) to study the role of LGR5$^+$ cells in the lung. We show that in pigs, like humans, there are two roles for LGR5$^+$ cells in homeostasis and development. In the developing lung, epithelial expression of LGR5 is tightly coupled with elongating bud tips and is only present during prenatal development. On the other hand, in the developing and postnatal lung, LGR5 expression defines a mesenchymal cell surrounding the airways. Using the pig model, we report the

unique 3D spatial arrangement of each population and a potential role for LGR5 in epithelial regeneration. We moreover define the role of the mesenchymal population as a niche for the airway basal stem cells and a mesenchymal stem cell subset closely associated with nerve fibers.

This model provides a new avenue for examining at least two key lung cell populations which need to be studied more for their potential role in orchestrating airway damage repair, contribution to fibrosis, or in forging lung repair and regeneration.

Results

Distinct and dynamic expression of LGR5 in developing lung bud tips and peri- airway mesenchymal cells.

To understand the spatial distribution of LGR5 expression throughout development and homeostasis, we used a transgenic porcine model expressing H2B-GFP under the control of the endogenous *LGR5* promoter, generated as previously described (15). In cryosections imaged by confocal microscopy, co-staining fetal lungs with EpCAM for epithelial cells and vimentin for mesenchymal cells shows that in the fetal lung, two LGR5$^+$ populations exist: one mesenchymal, surrounding all of the airways, and one epithelial, found in the bud tips (Figure 1A-C). In postnatal lung, only the LGR5$^+$ mesenchymal population is present, surrounding airways of all sizes, and occupying a sub-basal position, directly adjacent to the airway epithelium (Fig 1D-F). For spatial mapping of the LGR5-expressing cells, we used the tissue clearing technique (16) and light sheet microscopy to acquire 3D images of fetal developmental day 80 (GD80) and juvenile porcine lungs (Supplementary Video). In the fetal lungs, LGR5 expression is robust surrounding both proximal and distal airways, and additionally is present in developing bud tips (Figure 1G). The postnatal lung, in contrast, solely expresses the population surrounding the airways (Figure 1H). In addition, to determine whether the distribution of LGR5 in the developing and postnatal pig lungs is representative of the human, we employed fluorescent *in situ* hybridization (FISH) to detect *LGR5* mRNA transcripts in human fetal and adult lung tissue. *LGR5* expression is robust in human developing lung bud tips (Figure 1I), with an almost identical pattern of expression as the pig (as in 1C). In addition, *LGR5* expression was detected in the subepithelial population surrounding maturing airways in the developing lung, as shown with co-staining with SCGB3A2, a marker of developing airway epithelium (Figure 1J). Finally, robust detection of *LGR5* is evident surrounding adult airways (Figure 1K). These data support that there are at least two distinct LG LGR5$^+$ populations present in human lung development and homeostasis, and that their presence is consistent in humans and pigs but differs largely from what has been reported in the mouse (9).

Transient and conserved expression pattern of LGR5 in human and pig fetal epithelial population in developing lung bud tips

We next asked what is the role of epithelial LGR5$^+$ population, which is present in the developing, but not adult, lung. We compared expression of LGR5 with well-established markers of bud tips, including SOX9 and SFTPC (17), as well as a marker for more developed airway cells, SOX2
(18). Interestingly, the pattern of LGR5 expression in developing bud tips appears to be somewhat stochastic, with LGR5$^+$ cells intercalated within the SOX9 cells throughout the lung bud tips (Figure 2A, 2D and 2I). Quantification of the proportion of LGR5$^+$ epithelial cells that express SOX2 shows that they are co-expressed significantly more in the pseudoglandular stage (gestational day 50, GD50) than in the canalicular stage (GD80), where there is almost no overlap between the two populations (Figure

2G) ($P<0.05$). In contrast, all LGR5$^+$ epithelial cells also express SOX9, at both GD50 and GD80 (Fig 2H). When examining the proportion of SOX9$^+$ cells that also express LGR5, approximately 42% of SOX9$^+$ bud tip cells also expressed LGR5 at GD50, but by GD80 that number is reduced to 22.2% (Figure 2H)($P<0.05$). Combined, these results suggest that epithelial LGR5 expression is increasingly restricted throughout development. Moreover, RSPO2, a known ligand of LGR5, is detectable in the developing bud tip region near LGR5 cells at both GD50 (Figure J-K) and GD80 (Figure 2L-M). LGR5 expression is also correlated with SFTPC expression in the bud tips, confirming that the epithelial LGR5 expression is specific to bud tips (Figure N-O red arrow), while the mesenchymal population does not express SFTPC (Figure 2O, white arrow). Thus, LGR5 expression is consistent and robust throughout bud tips, but the pattern of expression throughout development is complex and more work needs to be done to determine the importance of the variation in expression.

For an initial high-resolution transcriptome analysis of LGR5$^+$ epithelial cells, we performed a scRNAseq screen on fluorescence-activated cell sorting (FACS) sorted fetal lung LGR5$^+$ (H2B- GFP positive) cells from GD80, a stage where both mesenchymal and epithelial cell populations are both present. We identified a total of 14 cell clusters comprising two main populations separated by EpCAM expression (Supplementary Figure 1) and identified key genes that can be used to characterize and relate each population to established human developmental populations. Among the four EpCAM$^+$ cell types, expression patterns of bud tip progenitors (*SFTPC, SFTPB, ETV4* and *ETV5)*, as well as other known markers of bud tip-adjacent stalk region and/or genes known to impact lung development such as *FOXA2, FOXP2* and *NGFR* (Supplement Figure 1), differed. Cluster Epi 4, for instance, likely represents a more differentiated cell type, with increased expression of the basal cell markers *NGFR, KRT5*, and *KRT14*, and reduced expression of *SFTPB, SFTPC* and *ETV5*, all known lung tip progenitor markers. Mesenchymal populations are more complex and will be described in further detail below. In addition, we used the scRNAseq data to identify genes differentially upregulated in LGR5 epithelial cells by comparing the transcriptome of the epithelial (based on EpCam expression) versus the mesenchymal sub clusters. Gene ontology biological process (BP) enrichment shows that LGR5$^+$ epithelial cells are highly enriched for developmental processes including tube development and tissue morphogenesis, and for molecular function (MF) they are highly significant for binding activity to actin, cadherin, and others (Supplementary Figure 2).

Functional analysis of fetal and adult epithelial cells via organoid modeling shows LGR5 expression is reactivated in vitro and is associated with organoid forming efficiency and cell fate

Since we established that the expression of LGR5 was increasingly restricted in the epithelial population between GD50 and GD80 we next asked whether LGR5 expression and developmental stage impacted their ability to form organoids. LGR5$^+$ or LGR5$^-$ epithelial cells were sorted from fetal GD50 or GD80 lungs and plated in 3D culture. In the given culture conditions, LGR5$^+$ cells from GD50 organoids formed significantly more organoids than any other group, while there was altogether low organoid formation from GD80 (Figure 3A). Overall, this suggests changes in cell state during development, where the LGR5$^+$ bud tip cells respond differently to inductive signals depending on the stage of development.

In addition, postnatal airway epithelial cells, which do not express LGR5, were seeded under the same conditions as the fetal cells. Surprisingly, after 5-7 days in culture, some organoids displayed few visually detectable LGR5$^+$ cells (Figure 3B), and by day ten, approximately greater than 10% of all cells

were LGR5$^+$. We next asked if there were any differences between the behavior of organoid-derived LGR5$^+$ and LGR5- cells. After dissociation, the LGR5$^+$ and LGR5- populations were sorted using fluorescence activated cell sorting (Figure 3B) and re-seeded in matrigel. We observed no detectable difference between the two populations in organoid forming efficiency, and organoids from the LGR5- population once again reactivated LGR5 (Figure 3C).

To ask more specifically which cells were reactivating LGR5 expression and forming organoids, we plated sorted lung cells based on NGFR, a known basal cell marker, and EpCAM (Figure 3D). The EpCAM$^+$/ NGFR$^+$ basal cell population formed significantly more organoids per well at the same concentration than the EpCAM$^+$/NGFR$^-$ cells (Figures 3D-E), but both expressed LGR5 and had mixed LGR5$^+$ and LGR5- organoids, suggesting that, although NGFR$^+$ basal cells were the primary driver of organoid formation, the basal cells and non-basal cells had the same fate under these conditions.

This led us to ask what the cell state of the LGR5$^+$ cells is by RNAseq analysis (Figure 3F). Among the top significantly upregulated genes in the LGR5$^+$ population were *SFTPC* and *AXIN2*, both markers of club/secretory cells or specialized progenitor AT2 cells (19), which are also co- expressed in LGR5$^+$ cells in bud tip development. In addition, LGR5$^+$ cells upregulated *BMP4*, *BMPR1B* and *TGFB2*, all known regulators of lung airway development (20). Among the genes downregulated in LGR5$^+$ cells were *AQP5*, an alveolar AT1 cell marker (21) *LTF*, a marker for differentiating basal cells (22) and *FRZB, FZD6* and *FST*, known negative regulators of canonical WNT signaling (23–25).

Given the shared markers of LGR5$^+$ organoid cells with lung development markers, we hypothesized that the LGR5 expression was related to cell fate. To test this, we altered the media conditions from a bronchioalveolar fate (dense, irregular shape with mix of basal and alveolar progenitors) to a bronchiolar phenotype (smooth, round shape, primarily basal cell progenitors) by removing WNT and WNT agonist CHIR signaling. After ten days in culture, none of the bronchiolar organoids expressed LGR5, while the bronchioalveolar controls were bright with H2BGFP expression (Figure 3G). To confirm the phenotype of each condition, we examined expression of KRT14 (basal cell marker) and SFTPC as previously described (26) (Figure 3H). This suggests LGR5 is only expressed when cells are differentiating toward an alveolar fate, but not when they maintain a basal cell state.

LGR5-expressing mesenchymal cells form a unique niche in peri-bronchiolar region and expresses a stromal cell gene signature

Next, we shifted to analysis of mesenchymal LGR5 expression. In postnatal lungs, since myofibroblasts are a known mesenchymal population surrounding airways, we asked if LGR5$^+$ cells were αSMA$^+$ myofibroblasts. As shown in Figure 4A-F, LGR5$^+$ and αSMA$^+$ populations remain separate; in proximal airways the LGR5$^+$ cells are located between the αSMA cells and the airway epithelial cells (Figure 4B-C), and in the distal bronchioalveolar region the two populations are intercalated surrounding the basal layer (Figure 4E-F), suggesting separate but

co-existing roles for αSMA$^+$ and LGR5$^+$ populations. This is further demonstrated by a 3D reconstruction of a proximal airway showing how the LGR5 and αSMA are also arranged in perpendicular orientation to each other (Figure 4G-H). Furthermore, the mesenchymal LGR5$^+$ cells are located directly adjacent to the NGFR$^+$ basal cells, separated by the airway epithelium basal membrane (Figure 4I). We also noted that at GD80, a stage that encompasses well developed proximal airways to elongating distal lung buds, the distribution of the LGR5$^+$ cells differed between

proximal and distal airways with the degree of spatial organization both longitudinally and circumferentially decreasing proximally to distally (Figure 4J-L).

As the LGR5$^+$ cells occupy a niche directly adjacent to the airway basal cells, and since LGR5 is a known potentiator of WNT signaling, we asked which genes were significantly enriched in the LGR5$^+$ population by comparing the transcriptome of LGR5$^+$ and LGR5$^-$ adult mesenchymal cells (Figure 4M-N). In examination of the WNT signaling pathway, LGR5$^+$ cells only express non- canonical WNT signals, such as *WNT5A*, *WNT9A, RYK, ROR1, ROR2, and GPC4*, in addition to known negative regulators of WNT signaling, such as *SFRP1, SFRP4, PRICKLE1, PRICKLE2* and *NKD1*. Furthermore, they upregulate WNT self-responsive signals such as *FZD1, FZD2, FZD7*, and *AXIN2* (Figure 4M). This suggests that the LGR5$^+$ cells are themselves actively responding to canonical WNT signaling, but that they are inhibiting canonical WNT signaling from reaching other cells in the niche, such as the adjacent basal cells which require a low-WNT environment (27). We also examined TGFBeta pathway genes as they are known to be involved in lung development and disease (28, 29) and interact with the WNT pathway (30, 31). As shown in Figure 4N many of the upregulated genes including *TGFB2, TGFB3, TGFB2R, BMP4*, and *BMP7* are known to be involved in lung development and/or function (32) as well as lung adenocarcinoma (33). *FGF10* and *FGFR1*, both known to play a central role in lung development and homeostasis (34, 35) are similarly over expressed in the LGR5$^+$ mesenchymal cells (Supplement Table 1). Additionally, significantly expressed genes were evaluated by Gene Set Enrichment Analysis (GSEA, Broad Institute). Comparisons to annotated cell types in the database reveal the ten most significantly enriched subsets, seven of which are stromal cell subsets (Figure 4P). Gene Ontology enrichment analysis also identified several significant organ and tissue morphogenesis and development biological processes as well as neuron development and differentiation with remarkable similarities between fetal and adult LGR5$^+$ cells (Supplementary Figure 3).

Lung mesenchymal LGR5+ cells have multilineage differentiation potential and serve as a signaling niche for airway basal cells

Since the postnatal LGR5$^+$ lung population shared a gene signature with many stromal cell and mesenchymal stem cell populations (Figure 4N), we next asked whether the LGR5$^+$ lung cells present functional properties of mesenchymal stromal and niche cells. When cultured *in vitro* LGR5$^+$ mesenchymal lung cells could differentiate into osteocytes, adipocytes, and chondrocytes (Figure 5A-D), which defines them as a mesenchymal stem cell subset. Because stromal cells generally define a support niche for other stem cell subsets, we hypothesized that the LGR5$^+$ cells designate the support niche for airway epithelium. To test this, we isolated NGFR$^+$ basal cells from lung airways and co-cultured at a 1:1 ratio with LGR5$^+$ mesenchymal cells in a matrigel dome with or without growth factors (Figure 5E). Remarkably, the LGR5$^+$ cells alone could support organoid formation from basal cells without additional growth factors. Furthermore, we noticed that the organoids in the LGR5$^+$ co-culture wells and growth factor only wells differed morphologically and were reminiscent of bronchiolar and bronchioalveolar organoids described in Figure 3G. Quantification of organoid type as previously described (26) shows that the presence of the growth factors induced a bronchioalveolar fate, but LGR5$^+$ mesenchymal stem cells in basic media supported the growth of bronchiolar organoids, and more specifically KRT14$^+$ basal cells (Figure 5F-G).

LGR5 mesenchymal cells are closely associated with nerve fibers and share markers of nerve

associated fibroblasts

Based on results of the RNAseq analysis showing significant enrichment of LGR5$^+$ mesenchymal cells for GO biological processes associated with neuronal development (Supplementary Figure 3A and 3D), and the known presence of nerves in proximity to the airways, we also examined the relationship between LGR5 and expression of PGP9.5, a pan-neuronal marker that has been shown to label nerve fibers in both adult and fetal lungs of multiple species including mice, pigs and humans (36–40) and S100B, a pan-astrocyte markers expressed in glial cell precursors (41, 42). We show that LGR5 mesenchymal cells at both fetal and adult stages are organized around PGP9.5 nerve fibers (Figure 6A-D and Figure 6H-K), and express S100B (Figure E-G and Figure L-N)

Due to its close association with the nerve fibers, as well as expression of S100B, we hypothesized that the LGR5$^+$ cells would share gene signatures with nerve associated fibroblasts (43). To test this, we examined lung, sciatic and peripheral nerve scRNAseq datasets from both mouse and human, as well as previously reported canonical markers of nerve associated cells (10, 43–51). Using these data, we compiled a set of markers defining the different nerve fiber- associated cell types (Supplement Table 2). Our differential gene expression data from postnatal lung shows that LGR5$^+$ cells are highly enriched for markers associated with epineural and endoneurial fibroblasts (Figure 6O) but not with Schwann cells or perineural cells (Figure 6P). These similar gene signatures, as well as the spatial colocalization, suggest that the LGR5$^+$ mesenchymal stem cells may also have a direct role in communicating with and/or maintaining the nerve fibers, in addition to their signaling to the basal airway cells.

Discussion

Here, we show that the pig is an excellent model for determining the role of the LGR5$^+$ cells in the lung and the importance of two separate populations throughout development and homeostasis. While the two described cell populations are consistent in humans (8,10) and pigs, it is unclear why the results are not consistent with mice. Lgr5 is reported in alveolar fibroblasts in mice, and the roles of the murine Lgr6$^+$ cells seem to be more akin to the LGR5$^+$ human and pig populations (9), given that they surround and support the airway niche. However, the murine Lgr6$^+$ population overlaps significantly with the α-SMA$^+$ population in the mouse, whereas the two populations are mutually exclusive in the pig. It is difficult to determine if the differences between the species are due to the differences in anatomy–the size of the airways and associated physiology, or if the redundant function of LGRs allows for interchangeable gene function across species.

Our *LGR5- H2B-GFP* reporter model also shows that LGR5 is heterogeneous in bud tip cells. Currently we do not know the mechanisms that drive such heterogenous expression pattern of LGR5 in SOX9-expressing multi-potent bud tip progenitors (52). In the epithelial LGR5$^+$ populations, the GO pathways suggest a strong relationship between the LGR5$^+$ cells and anchoring in the ECM. That, combined with their position in the bud tips, which is increasingly restricted throughout development, and previous reports in the intestinal crypts that LGR5 itself is correlated with anchoring in a niche (53), suggests that LGR5 may be important for anchoring the cells in the niche and maintaining an undifferentiated state as the bud tips elongate throughout development. The presence of LGR5 in the bronchioalveolar organoids suggests that this transient pathway may be reactivated during regeneration.

In the mesenchymal population, we identify an airway specific fibroblast population separate from myofibroblasts that is present at homeostasis and define their role as a mesenchymal stromal cell and

a support niche cell for basal cells. Interestingy, our RNAseq data from LGR5$^+$ mesenchymal stem cells show that they secrete canonical WNT inhibitors and upregulate WNT receptors and downstream WNT pathways. Their unique position surrounding the basal cells suggest that the LGR5$^+$ mesenchymal cell may play an active role in blocking ambient WNT signaling from lung interstitium from reaching the airway. Recent work shows that canonical WNT inhibitors promote basal cell stemness (54), while increased canonical WNT signaling promotes basal cell proliferation in airway repair (55). This is evidence that LGR5$^+$ cells may directly control airway basal cell homeostasis and proliferation by titration of WNT signaling.

More work must be done to determine how the signaling of the LGR5$^+$ mesenchymal cells is impacted by their close association with the nerve fibers. There are reports of innervation impacting airway branching during development (56), epithelial organ regeneration (57) and being involved in diseases such as asthma and cystic fibrosis (58), yet there is little known about the mechanism by which nerve signals impact airway function. The neural/mesenchymal/epithelial niche we report here is highly reminiscent of the enteric glia network present in the gastrointestinal tract (59), which has recently been shown to regulate the intestinal stem cell niche through a complex glial cell network (60). Some studies have also shown activation of a transcriptional injury signature in lung nerves after lung damage (61), which could impact their signaling with the LGR5$^+$ cells in injury.

Overall, this work represents multiple exciting developments toward the understanding of lung cell dynamics and offers a new model for functional studies of LGR5$^+$ lung cell populations.

Methods

Transgenic porcine tissue

All experiments were carried out in strict accordance with the Institutional Animal Care and Use Committee of North Carolina State University (IACUC protocol 17-028-B), and followed the established ARRIVE guidelines (62). LGR5-H2B-GFP transgenic pigs were generated by somatic cell nuclear transfer as previously described (63). Male and female transgenic offspring of the clones were used in these experiments, with no detectable differences. Experiments in this study are performed using lung tissue from six juvenile or adult pigs, five fetal GD80 fetuses, five fetal GD50 fetuses and one PD111 postnatal. Data are representative of both sexes. Human lung tissues were acquired from sub-transplant-quality lungs from donors without pre-existing lung disease and obtained from the Marisco Lung Institute at the University of North Carolina at Chapel Hill (University of North Carolina Biomedical Review Board 03-1396). De-identified human fetal lung tissue sections were obtained from Duke Biorepository & Precision Pathology Center (BRPC). All research using this human fetal lung tissue was approved by the Duke University Institutional Review Board.

Tissue Clearing

Here, we used the BoneClear procedure for clearing the porcine lungs with some adjustments; Perfusion, decalcification, and agarose embedding steps were not conducted, and immunostaining occurred over 7 days with anti-GFP primary antibody (Aves Labs, GFP-1010), and Cy3 donkey anti-Chicken IgG (Jackson Immuno Research Labs, 703165155) .We used a custom light-sheet microscope (64) to image the cleared lungs. The sample was mounted inside a custom chamber (aluminum and glass) to be immersed in 100% dibenzyl ether. A silicone membrane was employed in front of the objective lens (10×/numerical aperture (NA) 0.6, Olympus; XLPLN10XSVMP-2) to minimize the potential damage to the objective lens when immersed in 100% dibenzyl ether. The working distance of the detection objective and the field of view was 8 mm and 1.77 mm^2, respectively.

Immunofluorescence

Porcine lung tissue was fixed in 4% paraformaldehyde at 4°C overnight and dehydrated in 30% sucrose before being embedded in OCT. Organoids were fixed in 2-4% paraformaldehyde and embedded in OCT or stained and imaged as whole mounts. Tissue or organoids were sectioned using a cryostat set to 20 µM. For immunofluorescent analysis, sections were blocked with 0.4% Triton X-100 and IHC/ICC blocking buffer (Invitrogen) followed by incubation of primary antibody for 1.5 hours at room temperature or 4°C overnight. Primary antibodies were applied at a 1:200 ratio; anti-KI67 (Invitrogen, MA5-14520), anti-EpCAM (Abcam, ab71916), anti-SOX9 (eBioscience, 14-9765-82), anti-SOX2 (Abcam, ab97959), anti-Alpha-Smooth Muscle Actin (Invitrogen 14-9760-82), anti-Vimentin (Santa Cruz, sc-6260), anti-PDGFRa (Bioss, BSM- 52829R), anti-Prosurfactant Protein C (Abcam, ab90716), SCBG3A2 (Abcam, ab181853). Sections were incubated with secondary antibodies Alexa Fluor 594 Goat Anti-Rabbit (Invitrogen, A-11012) and Alexa Fluor 647 Goat Anti-Mouse (Invitrogen, A-21236) at a 1:500 ratio for 1 hour at room temperature and mounted with Prolong Diamond Antifade Mount with DAPI. Slides were imaged with an Olympus Fluoview 3000 upright confocal microscope.

RNAscope *in situ* hybridization

RNAscope was performed according to the manufacturer's instructions (ACD Bio). Briefly, paraffin embedded lung tissue from human fetus or adult was sectioned at 7 µM. Slides were deparaffinized with xylene, then heat treated followed by protease digestion. The tissue was hybridized with custom probes targeting Hs-SCGB3A2 (544951) and Hs-LGR5 (311021-C2). A positive control probe against human (139-989 region) cyclophilin B or as a negative control, a probe targeting the bacterial gene dapB were tested. After chromogenic development, slides were washed and imaged by confocal microscopy.

Cell Isolation and Sorting

Cells were isolated from lungs of adult or fetal LGR5 pigs. 2-3 cm^2 pieces of lung were collected in cold PBS and moved into a sterile hood. Lung tissue was then minced using scissors or razor blade and then washed twice with cold PBS to remove blood and immune cells. Minced tissues were then incubated for 1 hour in a roller incubator at 37 in an enzymatic digest buffer containing 5 mg/mL Dispase (Invitrogen), 2 mg/mL DNase I (STEMCELL Technologies), and 5mg/mL (adult) or 2mg/mL (fetal) Collagenase Type II (Sigma). The digestion mixture was then strained using a 70 µM cell strainer and washed with a wash buffer (PBS, 5% FBS, 1% antibiotic-antimycotic) and centrifuged. For adult tissue, pellets were incubated in Red Blood Cell Lysis Buffer (Invitrogen) for 10 minutes at room temperature with gentle agitation. For fluorescent activated cell sorting, cells from porcine lung or dissociated organoids were suspended in MACS buffer (Miltenyi) and incubated with 10µl/ml anti-EpCAM-APC (Thermo Scientific, 17-5791-83) and/or anti-NGFR-PE (eBioscience, 12-9400-41). Propidium iodide was added for dead cell exclusion immediately before fluorescence activated cell sorting (Beckman Coulter MoFlo XPD).

Organoid Culture

For generation of juvenile and fetal lung organoids, 2 x 10^3 cells/droplet were mixed with 25 µl of Matrigel and pipetted as droplets on tissue culture plates. Droplets containing cells were allowed to solidify upside down at 37 for 20 minutes and then were overlaid with culture media, which was replaced every other day. Basic growth media consisted of DMEM/F12 (Life Technologies, 12634-010), Glutamax (Life Technologies, 35050-061), HEPES (Life Technologies, 15630-106), N-2 (Life

Technologies, 17502-048), B27 (Life Technologies, 12587-010), and 1% antibiotic- antimycotic (Gibco, 15240-096). Bronchioalveolar conditions consisted of LWRN-conditioned media (collected from ATCC CRL-3276) was mixed with basic media at a 1:1 ratio, and a growth factor master mix was added for final concentrations of CHIR99021 (PeproTech, 2520691) (5 μM), EGF (PeproTech, AF-100-15) (100 ng/ mL), Nicotinamide (Life Technologies, 17502-048) (2mM), LY2157299 (Cayman Chemical Company 15312) (1 μM), A-83-01 (2 nM), Y27632 (20uM), and FGF10 (16.6ng/mL). For bronchiolar conditions, no LWRN was added and the mastermix contained added R-Spondin (R&D Systems 4645RS/CF) (2 μg/mL), reduced CHIR99021(1 μM), EGF (100 ng/ mL), (Nicotinamide (2mM), LY2157299(1 μM), A-83-01 (2 nM),
Y27632 (20 μM), and FGF10 (16.6 ng/mL). For co-culture conditions, $LGR5^+$ mesenchymal cells were mixed at a 1:1 ratio with $NGFR^+$ airway cells (2,000 cells each) and resuspended in a 25 μL droplet of reduced growth factor Matrigel (Corning) overlaid with basic growth media. To dissociate organoids for passage or FACS, ice cold Matrigel Recovery Solution was used.

RNA sequencing analysis

For bulk RNAsequencing, each group was Ultra-low input RNA-seq. Library Preparation, and HiSeq Sequencing RNA library preparations and sequencing reactions were conducted at GENEWIZ, LLC. (South Plainfield, NJ, USA). For fetal samples, but not for postnatal or organoids, SMART-Seq v4 Ultra Low Input Kit for Sequencing was used for full-length cDNA synthesis and amplification (Clontech, Mountain View, CA), and Illumina Nextera XT library was used for sequencing library preparation. The final library was assessed with Agilent TapeStation. The sequencing libraries were multiplexed and clustered on a flowcell. After clustering, the flowcell was loaded on the Illumina HiSeq instrument according to the manufacturer's instructions. The samples were sequenced using a 2x150 Paired End (PE) configuration. Image analysis and base calling were conducted by the HiSeq Control Software (HCS). Raw sequence data (.bcl files) generated from Illumina HiSeq was converted into fastq files and de-multiplexed using Illumina's bcl2fastq 2.17 software. Sequence reads were trimmed to remove possible adapter sequences and nucleotides with poor quality using Trimmomatic v.0.36. The trimmed reads were mapped to the Sus scrofa reference genome available on ENSEMBL using the STAR aligner v.2.5.2b. The STAR aligner is a splice aligner that detects splice junctions and incorporates them to help align the entire read sequences. BAM files were generated because of this step. Unique gene hit counts were calculated by using feature Counts from the Subread package v.1.5.2. Only unique reads that fell within exon regions were counted. After extraction of gene hit counts, the gene hit counts table was used for downstream differential expression analysis. Using DESeq2 (v1.37.6), a comparison of gene expression between the groups of samples was performed. The Wald test was used to generate p-values and Log2 fold changes. Genes with adjusted p-values < 0.05 and absolute log2 fold changes > 1 were called as differentially expressed genes for each comparison. Gene set enrichment analysis was performed using GSEA (Broad Institute) (65, 66) and ClusterProfiler (67).

Single cell RNAsequencing and computational analysis

Single cell suspensions from GD80 fetuses were loaded into a Chromium Controller (10x Genomics) for gel beads in emulsion. After scRNA-seq library preparation with the Chromium SIngle Cell 3' Library & Gel Bead Kit, quality analysis was performed using a bioanalyzer. Libraries were sequenced using an Illumina NextSeq500 system (~400M repair pairs). Barcodes were deconvoluted into a cells x genes matrix using alevin v1.5.2 based on the Sus scrofa Ensembl v11.1.105 assembly, and these counts were imported into R (v4.2.0) for analysis with the Seurat package (v4.1.1) using the RStudio IDE (v2022.07.1). Cells with fewer than less than 5% ribosomal reads and 2000 detected genes were discarded. Unsupervised clustering of the cells was performed with Louvain-Jaccard clustering with multilevel refinement (algorithm=2) implemented in the FindClusters function in Seurat with a resolution

of 0.75. Visualizations were generated using the FeaturePlot function in Seurat with Uniform Manifold Approximation and Projection (UMAP) dimensional reduction. The Seurat FindAllMarkers function and Presto (v1.0.0) were used to identify marker genes of each cluster.

Quantification of SOX2/SOX9

Quantification of $SOX2^+$, $SOX9^+$, and $LGR5^+$ cells in fetal lung tissue was performed using ImageJ (NIH). Only epithelial cells were included in the calculations. For SOX2 and LGR5 coexpression, the number of nuclei that expressed both were calculated as a proportion of total $LGR5^+$ cell nuclei. For SOX9 and LGR5 coexpression, it was a proportion of coexpressing nuclei out of the total $SOX9^+$ cells. Statistical analysis comparing ratios of co-expressing cells between D50 and D80 sections was performed using a Welch Two Sample T-test in R, n=10 photos per group, representative of 2 different fetal lungs each.

Mesenchymal stem cell differentiation Assay

For adipogenesis and osteogenesis differentiation assays, $LGR5^+$, porcine bone marrow derived mesenchymal stem cells (BMSC) (positive control), and dermal fibroblasts (negative control) were seeded at a density of 50×10^3 cells in 12-well plates and cultured until confluent in a growth medium of DMEM (Corning 10-014-CV), 10% FCS, 1% Antibiotic Antimycotic (Corning 30-004- Cl). Differentiation conditions were performed as previously described (68–70). Briefly, for adipogenic differentiation, confluent cells were incubated with High Glucose DMEM (4.5 g/l glucose, Cytiva SH30081.01), 10% FCS, 1% antibiotic antimycotic, 1 µM dexamethasone, 0.5 µM isobutylmethylxanthine, 50 µM indomethacin, and 1% ITS premix (insulin-transferrin-selenium). For osteogenic differentiation, high glucose DMEM, 10% FCS, 1% antibiotic antimycotic, 0.5 µM dexamethasone, 0.17 mM ascorbic acid, 10 mM sodium β-glycerol phosphate. For chondrogenesis, 2×10^5 cells of each type were seeded into a 96-well, round bottom, non- adherent plate and cultured for one week in 200 µL of the growth medium for pellet formation. For chondrogenic differentiation, pellets were switched to a differentiation medium composed of High Glucose DMEM, 1% antibiotic antimycotic, 0.5 µM dexamethasone, 0.17 mM ascorbic acid, 1% ITS premix and 10 ng/ml transforming growth factor β1 (TGF-β1). After 4 to 6 weeks for each condition, cells were washed with PBS, then fixed in 2% PFA for 10 minutes followed by 4% PFA for 2 hours on ice. OilRedO, Alizarin Red S, and Alcian Blue were applied to detect adipogenic, osteogenic, and chondrogenic differentiation, respectively, and imaged on a Leica Compound Microscope.

Data and software availability

scRNA-seq data and Seurat objects generated in this study are available from the Gene Expression Omnibus (GEO) under accession code GSE218658. The code to process, analyze and visualize the sequencing data is available at https://github.com/RossLampe/Two_roles_of_LGR5_in_the_lung.

Author Contributions

KMP, NKG, JAP Conceived and designed the analysis

YM, RL, JC, AC, LE, KG Collected the data

AM, AG, JMS, PKM, AT, PRT Contributed data or analysis tools

KMP, YM, RL, JMS Performed the analysis

KMP, NKG, JAP Wrote the paper.

Declaration of Interest

The authors declare no competing interests.

Acknowledgments
This work was supported by awards F31AR077423 to KMP, T34GM131947 to AC, and R21OD019738 to JAP. Authors are grateful to staff at the Laboratory Animal Resources and the Central Procedures laboratories at the College of Veterinary Medicine, North Carolina State University. The single-cell RNA-seq project was facilitated by the Advanced Analytics Core (partially supported by garnet P30 DK034987) and by the Bioinformatics and Analytics Research Collaborative (BARC) at the University of North Carolina at Chapel Hill School of Medicine.

References

1. N. Barker, S. Tan, H. Clevers, Lgr proteins in epithelial stem cell biology. *Development* **140**, 2484–2494 (2013).

2. N. Barker, *et al.*, Identification of stem cells in small intestine and colon by marker gene Lgr5. *Nature* **449**, 1003–1007 (2007).

3. C. Leung, S. H. Tan, N. Barker, Recent Advances in Lgr5$^+$ Stem Cell Research. *Trends Cell Biol.* **28**, 380–391 (2018).

4. R. S. Kadzik, *et al.*, Wnt ligand/Frizzled 2 receptor signaling regulates tube shape and branch-point formation in the lung through control of epithelial cell shape. *Proc. Natl. Acad. Sci. U. S. A.* **111**, 12444–12449 (2014).

5. M. Hussain, *et al.*, Wnt/β-catenin signaling links embryonic lung development and asthmatic airway remodeling. *Biochim. Biophys. Acta Mol. Basis Dis.* **1863**, 3226–3242 (2017).

6. A. A. Raslan, J. K. Yoon, WNT Signaling in Lung Repair and Regeneration. *Mol. Cells* **43**, 774–783 (2020).

7. S. M. Bell, *et al.*, R-spondin 2 is required for normal laryngeal-tracheal, lung and limb morphogenesis. *Development* **135**, 1049–1058 (2008).

8. R. F. C. Hein, *et al.*, R-SPONDIN2$^+$ mesenchymal cells form the bud tip progenitor niche during human lung development. *Dev. Cell* (2022) https:/doi.org/10.1016/j.devcel.2022.05.010.

9. J.-H. Lee, *et al.*, Anatomically and functionally distinct lung mesenchymal populations marked by Lgr5 and Lgr6. *Cell* **170**, 1149–1163. e12 (2017).

10. P. K. L. Murthy, *et al.*, Human distal lung maps and lineage hierarchies reveal a bipotent progenitor. *Nature* **604**, 111–119 (2022).

11. M. A. Benahmed, *et al.*, NMR HRMAS spectroscopy of lung biopsy samples: Comparison study between human, pig, rat, and mouse metabolomics. *Magn. Reson. Med.* **71**, 35–43 (2014).

12. F. Meurens, A. Summerfield, H. Nauwynck, L. Saif, V. Gerdts, The pig: a model for human infectious diseases. *Trends Microbiol.* **20**, 50–57 (2012).

13. J. K. Lunney, *et al.*, Importance of the pig as a human biomedical model. *Sci. Transl. Med.* **13**, eabd5758 (2021).

14. E. P. Judge, *et al.*, Anatomy and bronchoscopy of the porcine lung. A model for translational respiratory medicine. *Am. J. Respir. Cell Mol. Biol.* **51**, 334–343 (2014).

15. K. M. Polkoff, *et al.*, LGR5 is a conserved marker of hair follicle stem cells in multiple species and is present early and throughout follicle morphogenesis. *Sci. Rep.* **12**, 9104 (2022).

16. Q. Wang, K. Liu, L. Yang, H. Wang, J. Yang, BoneClear: whole-tissue immunolabeling of the intact mouse bones for 3D imaging of neural anatomy and pathology. *Cell Res.* **29**, 870–872 (2019).

17. B. E. Rockich, *et al.*, Sox9 plays multiple roles in the lung epithelium during branching morphogenesis. *Proc. Natl. Acad. Sci. U. S. A.* **110**, E4456–64 (2013).

18. S. Danopoulos, *et al.*, Human lung branching morphogenesis is orchestrated by the spatiotemporal distribution of ACTA2, SOX2, and SOX9. *Am. J. Physiol. Lung Cell. Mol. Physiol.* **314**, L144–L149 (2018).

19. W. J. Zacharias, *et al.*, Regeneration of the lung alveolus by an evolutionarily conserved epithelial progenitor. *Nature* **555**, 251–255 (2018).

20. D. Warburton, *et al.*, Molecular mechanisms of early lung specification and branching morphogenesis. *Pediatr. Res.* **57**, 26R–37R (2005).

21. P. Flodby, *et al.*, Cell-specific expression of aquaporin-5 (Aqp5) in alveolar epithelium is directed by GATA6/Sp1 via histone acetylation. *Sci. Rep.* **7**, 3473 (2017).

22. P. Kadur Lakshminarasimha Murthy, *et al.*, Human distal lung maps and lineage hierarchies reveal a bipotent progenitor. *Nature* **604**, 111–119 (2022).

23. X.-P. Wang, *et al.*, Modulation of activin/bone morphogenetic protein signaling by follistatin is required for the morphogenesis of mouse molar teeth. *Dev. Dyn.* **231**, 98–108 (2004).

24. P. N. Kongkham, *et al.*, The SFRP family of WNT inhibitors function as novel tumor suppressor genes epigenetically silenced in medulloblastoma. *Oncogene* **29**, 3017–3024 (2010).

25. G. Naz, *et al.*, FZD6 encoding the Wnt receptor frizzled 6 is mutated in autosomal- recessive nail dysplasia. *Br. J. Dermatol.* **166**, 1088–1094 (2012).

26. J. J. Kathiriya, *et al.*, Human alveolar type 2 epithelium transdifferentiates into metaplastic $KRT5^+$ basal cells. *Nat. Cell Biol.* **24**, 10–23 (2022).

27. K. B. McCauley, *et al.*, Efficient Derivation of Functional Human Airway Epithelium from Pluripotent Stem Cells via Temporal Regulation of Wnt Signaling. *Cell Stem Cell* **20**, 844– 857.e6 (2017).

28. Q. Miao, *et al.*, Abrogation of mesenchyme-specific TGF-β signaling results in lung malformation with prenatal pulmonary cysts in mice. *Am. J. Physiol. Lung Cell. Mol. Physiol.* **320**, L1158–L1168 (2021).

29. S. K. Ahlfeld, J. Wang, Y. Gao, P. Snider, S. J. Conway, Initial Suppression of Transforming Growth Factor-β Signaling and Loss of TGFBI Causes Early Alveolar Structural Defects Resulting in Bronchopulmonary Dysplasia. *Am. J. Pathol.* **186**, 777–793 (2016).

30. T. Kadota, *et al.*, Human bronchial epithelial cell-derived extracellular vesicle therapy for pulmonary fibrosis via inhibition of TGF-β-WNT crosstalk. *J Extracell Vesicles* **10**, e12124 (2021).

31. X. Guo, X.-F. Wang, Signaling cross-talk between TGF-beta/BMP and other pathways. *Cell Res.* **19**, 71–88 (2009).

32. A. Saito, M. Horie, T. Nagase, TGF-β Signaling in Lung Health and Disease. *Int. J. Mol. Sci.*

19 (2018).

33. Z. Xu, C. Chen, Abnormal Expression and Prognostic Significance of Bone Morphogenetic Proteins and Their Receptors in Lung Adenocarcinoma. *Biomed Res. Int.* **2021**, 6663990 (2021).

34. T. Yuan, T. Volckaert, D. Chanda, V. J. Thannickal, S. P. De Langhe, Fgf10 Signaling in Lung Development, Homeostasis, Disease, and Repair After Injury. *Front. Genet.* **9**, 418 (2018).

35. T. Yuan, *et al.*, Temporospatial Expression of Fgfr1 and 2 During Lung Development, Homeostasis, and Regeneration. *Front. Pharmacol.* **11**, 120 (2020).

36. M. G. Drake, M. Cook, A. D. Fryer, D. B. Jacoby, G. D. Scott, Airway Sensory Nerve Plasticity in Asthma and Chronic Cough. *Front. Physiol.* **12**, 720538 (2021).

37. J. M. Lauweryns, L. Van Ranst, Protein gene product 9.5 expression in the lungs of humans and other mammals. Immunocytochemical detection in neuroepithelial bodies, neuroendocrine cells and nerves. *Neurosci. Lett.* **85**, 311–316 (1988).

38. M. P. Sparrow, M. Weichselbaum, P. B. McCray, Development of the innervation and airway smooth muscle in human fetal lung. *Am. J. Respir. Cell Mol. Biol.* **20**, 550–560 (1999).

39. M. Weichselbaum, A. W. Everett, M. P. Sparrow, Mapping the innervation of the bronchial tree in fetal and postnatal pig lung using antibodies to PGP 9.5 and SV2. *Am. J. Respir. Cell Mol. Biol.* **15**, 703–710 (1996).

40. G. D. Scott, E. D. Blum, A. D. Fryer, D. B. Jacoby, Tissue optical clearing, three- dimensional imaging, and computer morphometry in whole mouse lungs and human airways. *Am. J. Respir. Cell Mol. Biol.* **51**, 43–55 (2014).

41. H.-S. Kim, *et al.*, Schwann Cell Precursors from Human Pluripotent Stem Cells as a Potential Therapeutic Target for Myelin Repair. *Stem Cell Reports* **8**, 1714–1726 (2017).

42. T. Gonzalez-Martinez, P. Perez-Piñera, B. Díaz-Esnal, J. A. Vega, S-100 proteins in the human peripheral nervous system. *Microsc. Res. Tech.* **60**, 633–638 (2003).

43. D. Gerber, *et al.*, Transcriptional profiling of mouse peripheral nerves to the single-cell level to build a sciatic nerve ATlas (SNAT). *Elife* **10** (2021).

44. J. S. Toma, *et al.*, Peripheral Nerve Single-Cell Analysis Identifies Mesenchymal Ligands that Promote Axonal Growth. *eNeuro* **7** (2020).

45. J. Wolbert, *et al.*, Redefining the heterogeneity of peripheral nerve cells in health and autoimmunity. *Proc. Natl. Acad. Sci. U. S. A.* **117**, 9466–9476 (2020).

46. K. J. Travaglini, *et al.*, A molecular cell atlas of the human lung from single-cell RNA sequencing. *Nature* **587**, 619–625 (2020).

47. M. Weber, *et al.*, Alternative generation of CNS neural stem cells and PNS derivatives from neural crest-derived peripheral stem cells. *Stem Cells* **33**, 574–588 (2015).

48. M. Ramosaj, *et al.*, Lipid droplet availability affects neural stem/progenitor cell metabolism and proliferation. *Nat. Commun.* **12**, 7362 (2021).

49. E. Madissoon, *et al.*, A spatial multi-omics atlas of the human lung reveals a novel immune cell survival niche. *bioRxiv*, 2021.11.26.470108 (2021).

50. Y.-A. Chen, I.-L. Lu, J.-W. Tsai, Contactin-1/F3 Regulates Neuronal Migration and Morphogenesis Through Modulating RhoA Activity. *Frontiers in Molecular Neuroscience* **11** (2018).

51. H. Zhang, *et al.*, Single-nucleus transcriptomic landscape of primate hippocampal aging. *Protein Cell* **12**, 695–716 (2021).

52. D. Sun, *et al.*, SOX9 maintains human foetal lung tip progenitor state by enhancing WNT and RTK signalling. *EMBO J.*, e111338 (2022).

53. K. S. Carmon, *et al.*, LGR5 receptor promotes cell-cell adhesion in stem cells and colon cancer cells via the IQGAP1-Rac1 pathway. *J. Biol. Chem.* **292**, 14989–15001 (2017).

54. C. J. Aros, *et al.*, High-Throughput Drug Screening Identifies a Potent Wnt Inhibitor that Promotes Airway Basal Stem Cell Homeostasis. *Cell Rep.* **30**, 2055–2064.e5 (2020).

55. C. J. Aros, C. J. Pantoja, B. N. Gomperts, Wnt signaling in lung development, regeneration, and disease progression. *Commun Biol* **4**, 601 (2021).

56. D. V. Bower, *et al.*, Airway branching has conserved needs for local parasympathetic innervation but not neurotransmission. *BMC Biol.* **12**, 92 (2014).

57. S. M. Knox, *et al.*, Parasympathetic stimulation improves epithelial organ regeneration. *Nat. Commun.* **4**, 1494 (2013).

58. K. J. Audrit, L. Delventhal, Ö. Aydin, C. Nassenstein, The nervous system of airways and its remodeling in inflammatory lung diseases. *Cell Tissue Res.* **367**, 571–590 (2017).

59. H. J. Rosenberg, M. Rao, Enteric glia in homeostasis and disease: From fundamental biology to human pathology. *iScience* **24**, 102863 (2021).

60. M. B. Baghdadi, *et al.*, Enteric glial cell heterogeneity regulates intestinal stem cell niches. *Cell Stem Cell* **29**, 86–100.e6 (2022).

61. M. M. Kaelberer, A. I. Caceres, S.-E. Jordt, Activation of a nerve injury transcriptional signature in airway-innervating sensory neurons after lipopolysaccharide-induced lung inflammation. *Am. J. Physiol. Lung Cell. Mol. Physiol.* **318**, L953–L964 (2020).

62. C. Kilkenny, W. J. Browne, I. C. Cuthill, M. Emerson, D. G. Altman, Improving bioscience research reporting: The ARRIVE guidelines for reporting animal research. *J. Pharmacol. Pharmacother.* **1**, 94–99 (2010).

63. S. C. Walker, *et al.*, A highly efficient method for porcine cloning by nuclear transfer using in vitro-matured oocytes. *Cloning Stem Cells* **4**, 105–112 (2002).

64. A. Moatti, *et al.*, Three-dimensional imaging of intact porcine cochlea using tissue clearing and custom-built light-sheet microscopy. *Biomed. Opt. Express* **11**, 6181–6196 (2020).

65. A. Subramanian, *et al.*, Gene set enrichment analysis: a knowledge-based approach for interpreting genome-wide expression profiles. *Proc. Natl. Acad. Sci. U. S. A.* **102**, 15545– 15550 (2005).

66. V. K. Mootha, *et al.*, PGC-1α-responsive genes involved in oxidative phosphorylation are coordinately downregulated in human diabetes. *Nat. Genet.* **34**, 267–273 (2003).

67. G. Yu, L.-G. Wang, Y. Han, Q.-Y. He, clusterProfiler: an R package for comparing biological themes among gene clusters. *OMICS* **16**, 284–287 (2012).

68. M. C. Ciuffreda, G. Malpasso, P. Musarò, V. Turco, M. Gnecchi, “Protocols for in vitro Differentiation of Human Mesenchymal Stem Cells into Osteogenic, Chondrogenic and Adipogenic Lineages” in *Mesenchymal Stem Cells: Methods and Protocols*, M. Gnecchi, Ed. (Springer New York, 2016), pp. 149–158.

69. S. Koh, M. Purser, R. Wysk, J. A. Piedrahita, Improved Chondrogenic Potential and Proteomic Phenotype of Porcine Chondrocytes Grown in Optimized Culture Conditions. *Cell. Reprogram.* **19**, 232–244 (2017).

70. Y.-H. K. Yang, C. R. Ogando, C. Wang See, T.-Y. Chang, G. A. Barabino, Changes in phenotype and differentiation potential of human mesenchymal stem cells aging in vitro. *Stem Cell Res. Ther.* **9**, 131 (2018).

Supplementary Information

Supplementary Figures S1. Single cell RNA sequencing of GF80 fetal porcine LGR5+ populations confirm the presence of epithelial and mesenchymal LGR5 cells populations during development.

Supplementary Figures S2. Gene Ontology and Gene Set Enrichment Analysis. (GSEA) of fetal LGR5+ epithelial cells.

Supplementary Figures S3. Gene Ontology and Gene Set Enrichment Analysis. (GSEA) of fetal and adult LGR5+ mesenchymal cells.

Table S1. Top 100 Upregulated genes in $LGR5^+$ Adult mesenchymal cells
Table S2. Markers of nerve and nerve-associated cells
Video #1. Fetal and adult lung light-sheet microscopy

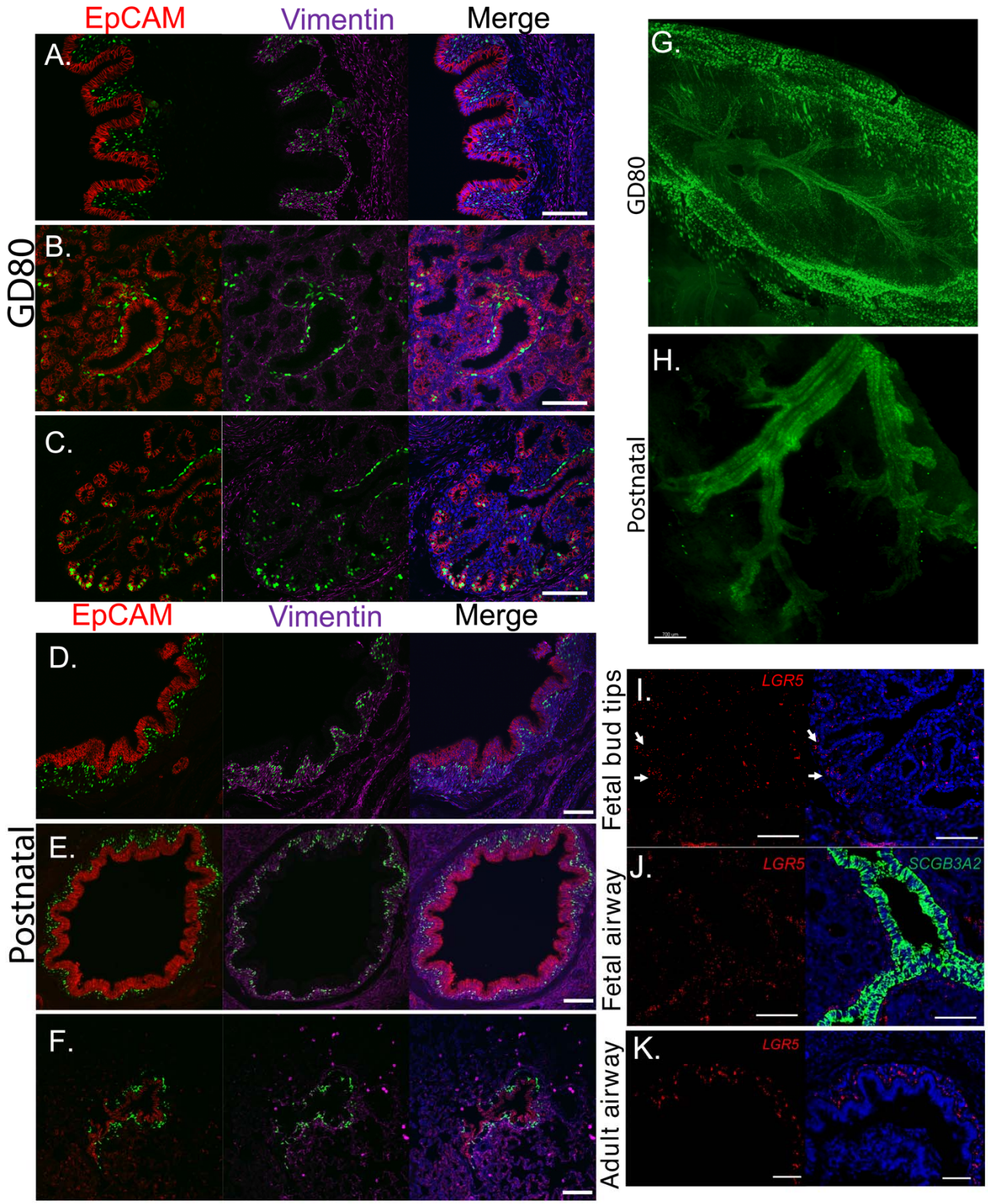
EpCAM
Vimentin
Merge
A.
B.
C.
GD80
G.
GD80
H.
Postnatal
EpCAM
Vimentin
Merge
D.
E.
F.
Postnatal
I.
LGR5
Fetal bud tips
J.
LGR5
SCGB3A2
Fetal airway
K.
LGR5
Adult airway

Figure 1. Two populations of LGR5-expressing cells in development and homeostasis in pigs and human lung. (A-C) In the GD80 lung, co-localization with EpCAM (red) or Vimentin (purple) shows that the population surrounding the airways is mesenchymal and surrounds developing large, mid and distal airways, while LGR5^{+} cells in the bud tips are EpCAM^{+} epithelial cells. (D-F) In the postnatal pig lung, the Vimentin^{+} mesenchymal population is present in airways of all sizes, and occupies the sub-basal space, but there is no LGR5 expression in epithelial cells. (G) 3D lightsheet microscopy of pig GD80 fetal lung showing LGR5 cells are an abundant population in the lung and surround the airways as well as being present in the developing bud tips. (H) In the postnatal lung, LGR5 is expressed only surrounding the airways. (I-K) Conservation of *LGR5* populations between humans and pigs. *In situ* hybridization with a probe detecting human *LGR5* transcripts in human developing lung shows the presence of epithelial *LGR5* expression in gestational day 135 bud tips (white arrows) (I), and the presence of the mesenchymal *LGR5*$^{+}$ expression in cells directly adjacent to the airway epithelium (stained with SCGB3A2) in both fetal day 142 (J) and adult (K) airways. Scale bars are equivalent to 100 μM.

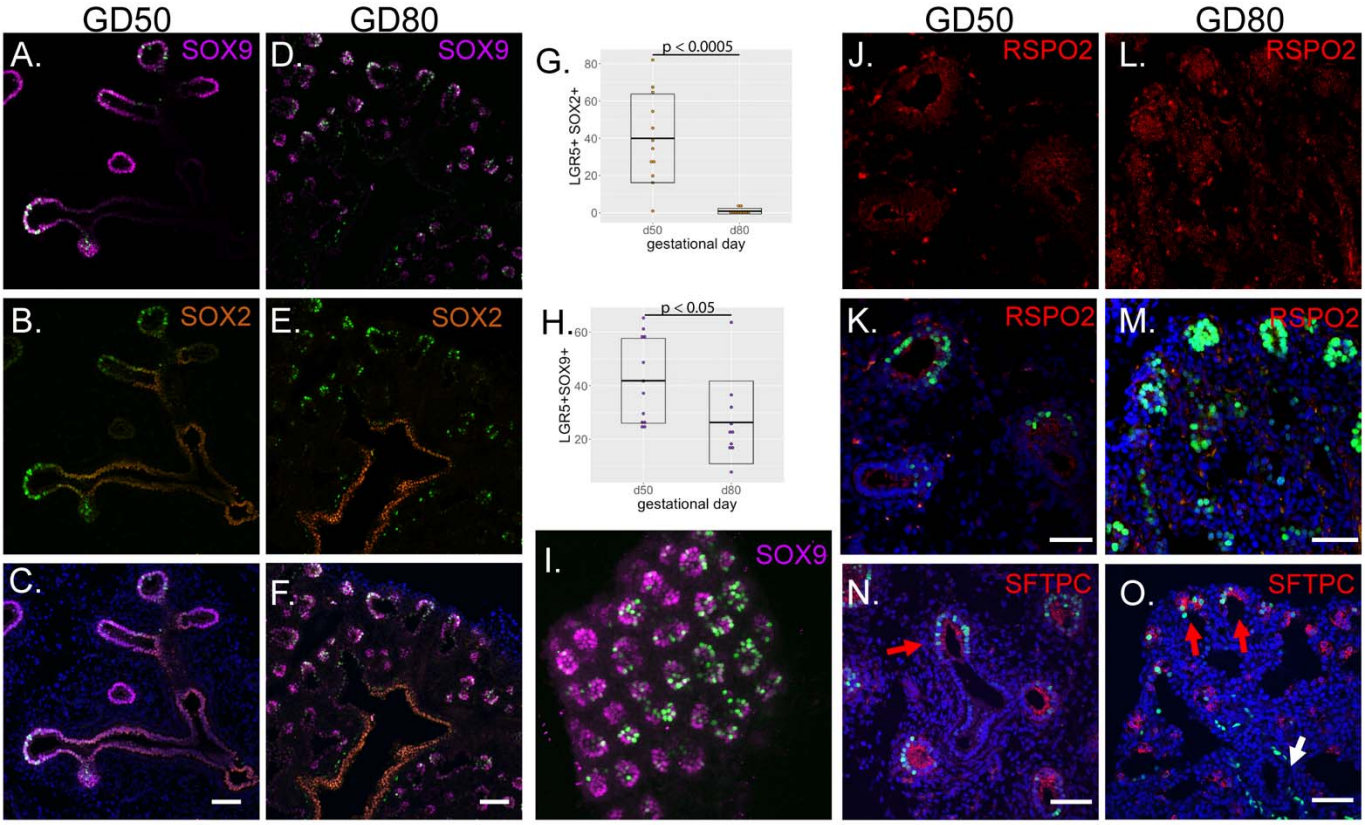

Figure 2. Epithelial LGR5 cells are spatially located in the distal portion of elongating lung bud and become more distally restricted as development progresses. (A-F) Representative images of the relationship between LGR5 and SOX9, a known marker of developing bud tips, and SOX2, a marker of more differentiated airways. (G) Quantification of LGR5 and SOX2 coexpression, represented as percentage of coexpressing cells over total LGR5$^+$ cells. Coexpression is significantly reduced between GD50 and GD80 ($p<0.0005$, Welch two sample t-test, n=10 images representative of sections from 2 different fetal lungs each). H) Percentage of LGR5$^+$ SOX9$^+$ as a proportion of total SOX9$^+$ cells decrease from GD50 to GD80 ($p<0.05$, Welch two sample t-test n=10 images, 2 different fetal lungs each). (I) 3D visualization of LGR5 and SOX9 expression at GD80 via whole-mount confocal imaging showing intercalated SOX9 and LGR5 expression in lung bud tips. (J-M) Expression of RSPO2 in the region surrounding bud tips. (N) GD50 fetal lung showing co-expression (red arrow) of LGR5 and the known lung bud tip marker SFTPC. (O) GD80 fetal lung showing co-expression of LGR5 and SFTPC in the lung bud epithelial cell (red arrow) but not the LGR5 mesenchymal cells surrounding the airways (white arrow). Statistical significance was established using a Welch two sample T-test.

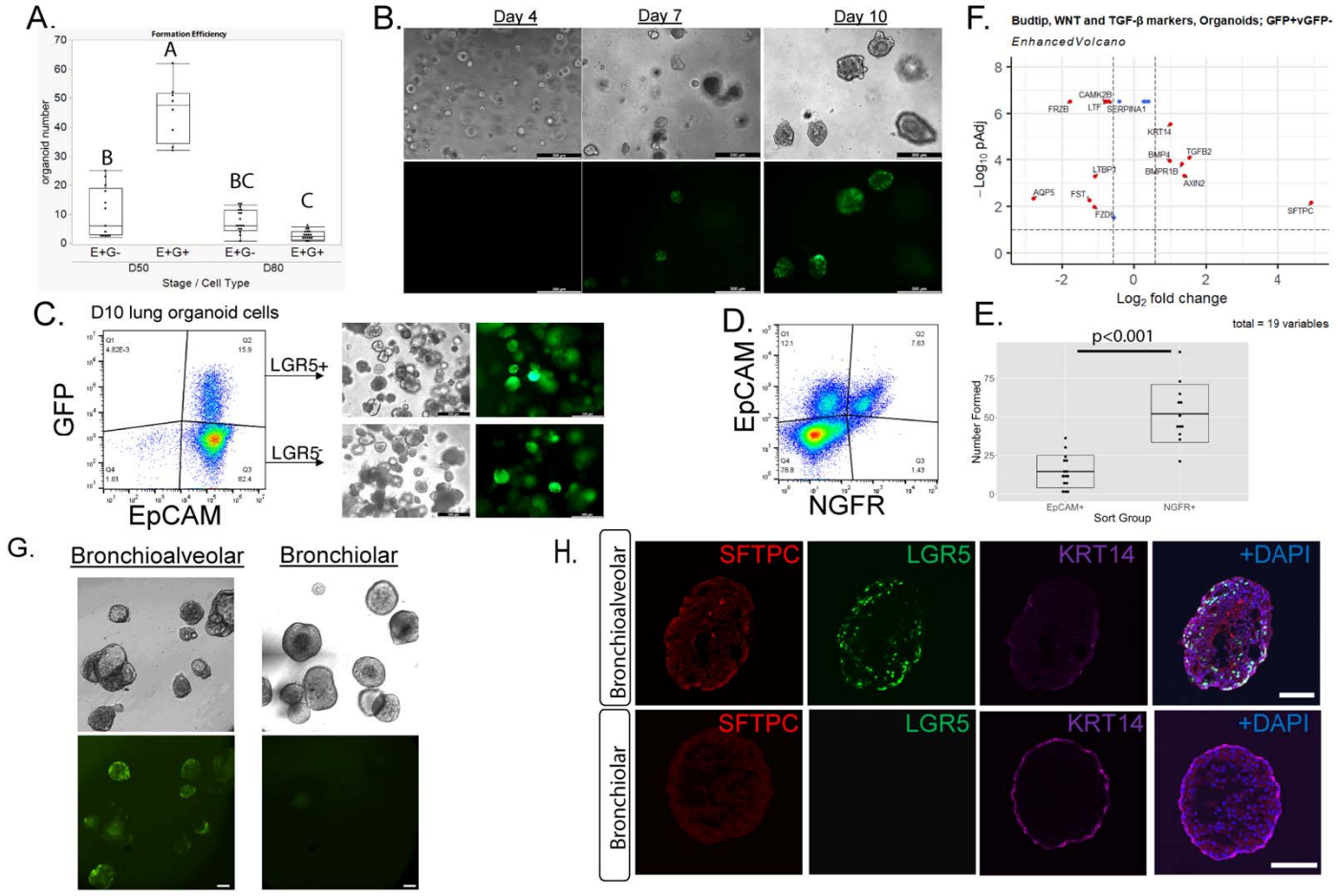

Figure 3. **LGR5 expression is transiently reactivated in adult epithelial organoids and is associated with organoid forming efficiency and cell fate.** (A) Organoid formation efficiency of EPCAM$^+$/LGR5$^+$ or EPCAM$^+$/LGR5- cells from GD50 or GD80 fetal pigs with GD50 EPCAM$^+$/LGR5$^+$ cells demonstrating the highest formation efficiency. Comparison of all pairs was performed using a one-way ANOVA by group, and comparison of means was performed by Tukey-Kramer HSD for all pairs, *n*=3 biological and 10 technical replicates for each group (B) EpCAM$^+$/ LGR5- cells from adult lungs were embedded in organoid culture. While organoids remained LGR5- after 4 days of culture, by 5-7 days LGR5 expression was detectable. By day 10, a mixture of LGR5$^+$ and LGR5- organoid could be detected. (C) After 10 days in culture, organoids were dissociated and sorted by EPCAM and LGR5-H2BGFP expression. EpCAM$^+$LGR5$^+$ and EpCAM$^+$LGR5- cells were plated separately for organoid formation, and both populations generated a mixture of LGR5 positive and negative organoids. Scale bar represents 100 uM(D) LGR5 adult lung cells were sorted based on expression of EpCAM and NGFR (an airway basal cell marker) and EpCAM$^+$/NGFR$^+$ and EpCAM$^+$/NGFR- cells were plated separately for organoid formation efficiency. (E) EpCAM$^+$/NGFR$^+$ epithelial cells formed organoids at a significantly higher efficiency than EpCAM$^+$/NGFR- cells ($p<0.001$, Welch two sample t-test, n=3 biological and 4 technical replicates each). (F) Organoid-derived LGR5$^+$ and LGR5- cells were sorted as in panel C and subject to RNA sequencing analysis. Differential gene expression of markers in the WNT and TGF-β signaling pathways are shown. LGR5$^+$ cells expressed markers of both bud tips (SFTPC) and basal cells (KRT14) in addition to upregulating BMP4 and TGFB2. (G) Postnatal epithelial cells were cultured in bronchioalveolar or bronchiolar organoid media and imaged by fluorescent or brightfield microscopy. Only bronchioalveolar culture conditions induced LGR5 expression. (H) Type of organoid (bronchiolar versus bronchioalveolar) was confirmed by morphology and by IHC using antibodies to SFTPC and KRT14. Scale bars represent 50 μM.

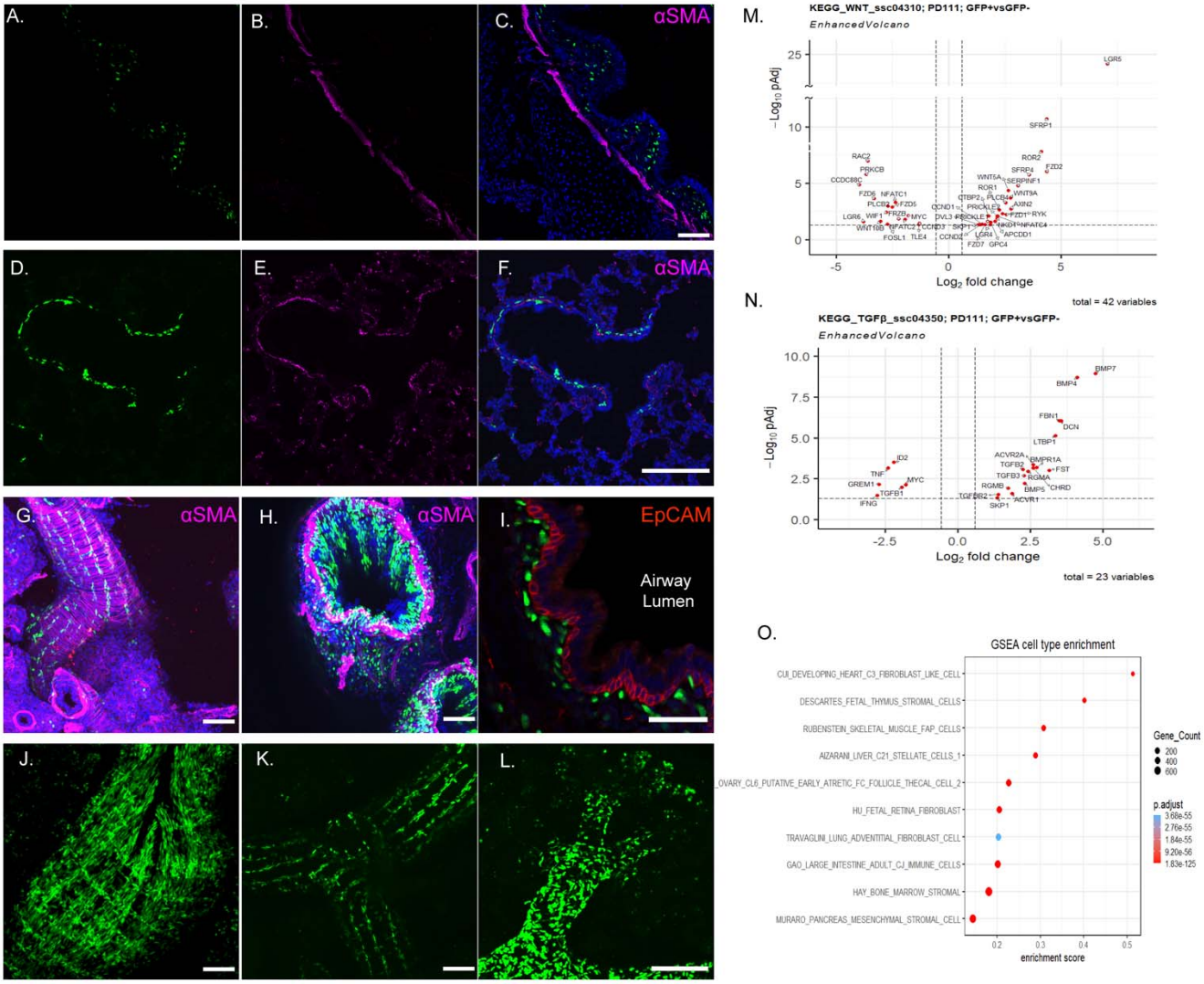

Figure 4. LGR5$^+$ mesenchymal populations are distinct from myofibroblasts, have a highly organized spatial distribution in the mature airways, lie in proximity to airway basal cells and have a unique transcriptional profile. (A-F) Confocal imaging of bronchiolar (A-C) and bronchioalveolar (D-F) cross-sections, shows that LGR5-H2BGFP cells are distinct from α-SMA expressing smooth muscle and myofibroblasts. In the mature airways LGR5$^+$ cells are located between the αSMA$^+$ layer and the lung airway epithelial cells, and in the distal airways/bronchioalveolar region, LGR5$^+$ and αSMA$^+$ are separate but closely positioned surrounding the airways. (G-H) 3D rendering of whole mount tissue shows the longitudinal arrangement of the LGR5$^+$ cells perpendicular to the orientation of the α-SMA$^+$ cells. (I) Close apposition between LGR5$^+$ cells and the basal airway epithelial cell identified by NGFR. (J-L) Spatial organization in GD80 whole mount confocal images, with both longitudinal and circumferential alignment in large proximal airways (I), primarily longitudinal alignment in smaller airways (J), and more random organization in distal airways near the elongating bud tips (K). Scale bar indicates 100 μM unless marked otherwise. (M) KEGG WNT and (N) KEGG TGFbeta pathways genes upregulated in postnatal (PD111) LGR5$^+$ cells. O) Gene set enrichment analysis for cell type (GSEA:C8) shows the top ten most similar cell populations in the database by transcriptome similarity.

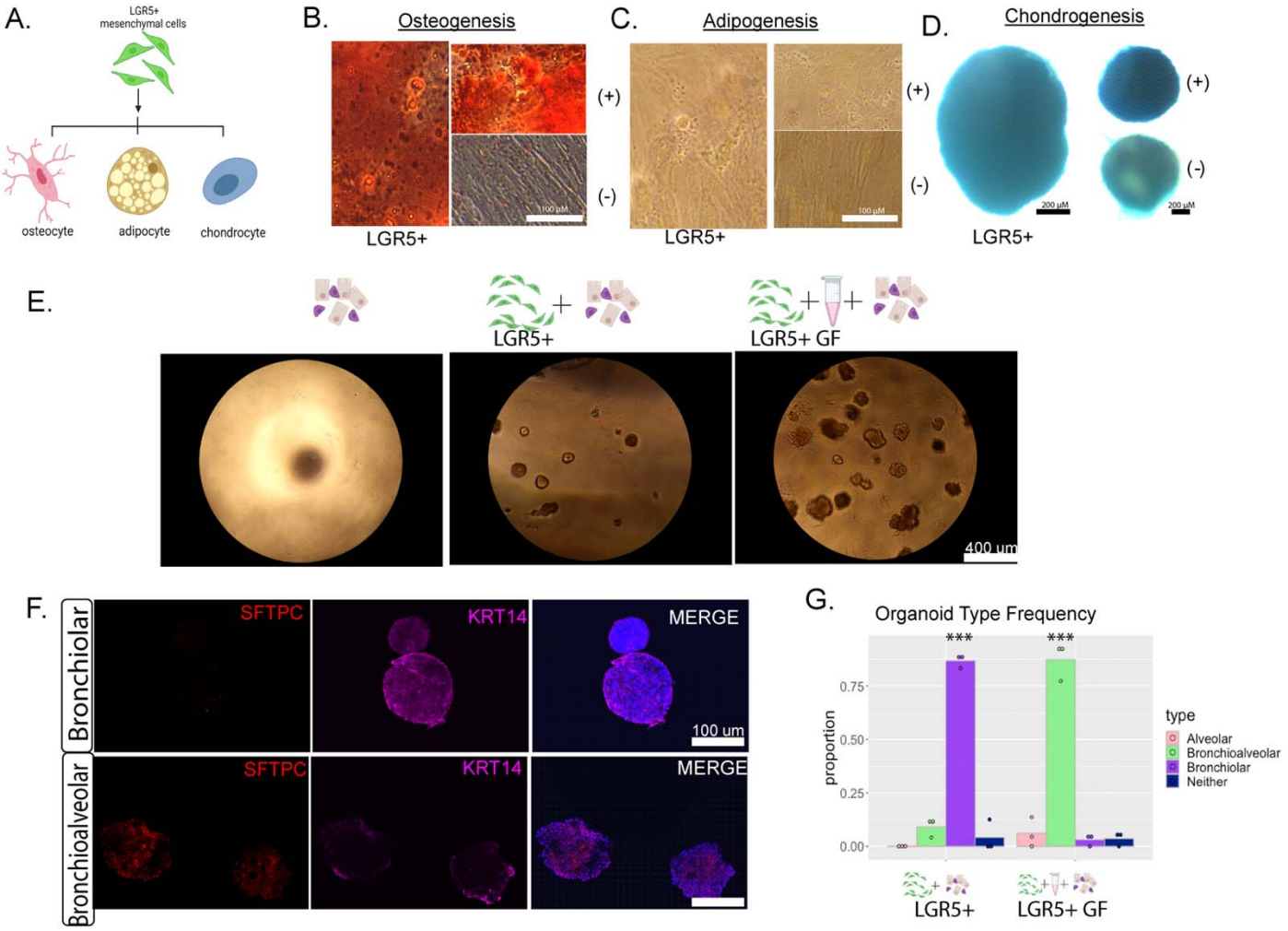

Figure 5. Postnatal LGR5$^+$ cells are mesenchymal stromal cells and support the airway basal cell niche. **(**A) LGR5$^+$ mesenchymal cells were cultured in osteocyte, adipocyte or chondrocyte differentiation media to examine whether they had multilineage properties. (B-D) LGR5$^+$ cells show the ability to differentiate into osteocytes (B), adipocytes (C), and chondrocytes (D). Porcine bone marrow mesenchymal stem cells were used as a positive control, and porcine dermal fibroblasts as negative controls. (E) Airway basal cells were seeded in growth factor deficient Matrigel either with no additional factors, in a 1:1 ratio with LGR5$^+$ mesenchymal cells only, or with 1:1 ratio of LGR5$^+$ mesenchymal cells and a growth factor cocktail. (F) Bronchiolar organoids were characterized by a spherical shape, robust expression of KRT14, and absence of SFTPC. Bronchioalveolar organoids had an irregular shape and expressed both SFTPC and KRT14. Representative images are shown. G) Proportion of organoid type for each growth condition. Organoids from epithelial cells co-cultured with LGR5$^+$ cells only were almost entirely bronchiolar, while conditions containing LGR5$^+$ cells and growth factors or growth factors alone yielded primarily bronchioalveolar organoids. *** indicates $p<0.005$, ANOVA for each treatment followed by pairwise t-tests to determine significant differences, points represent n= 3 biological replicates which each included at least 25 organoids per group.

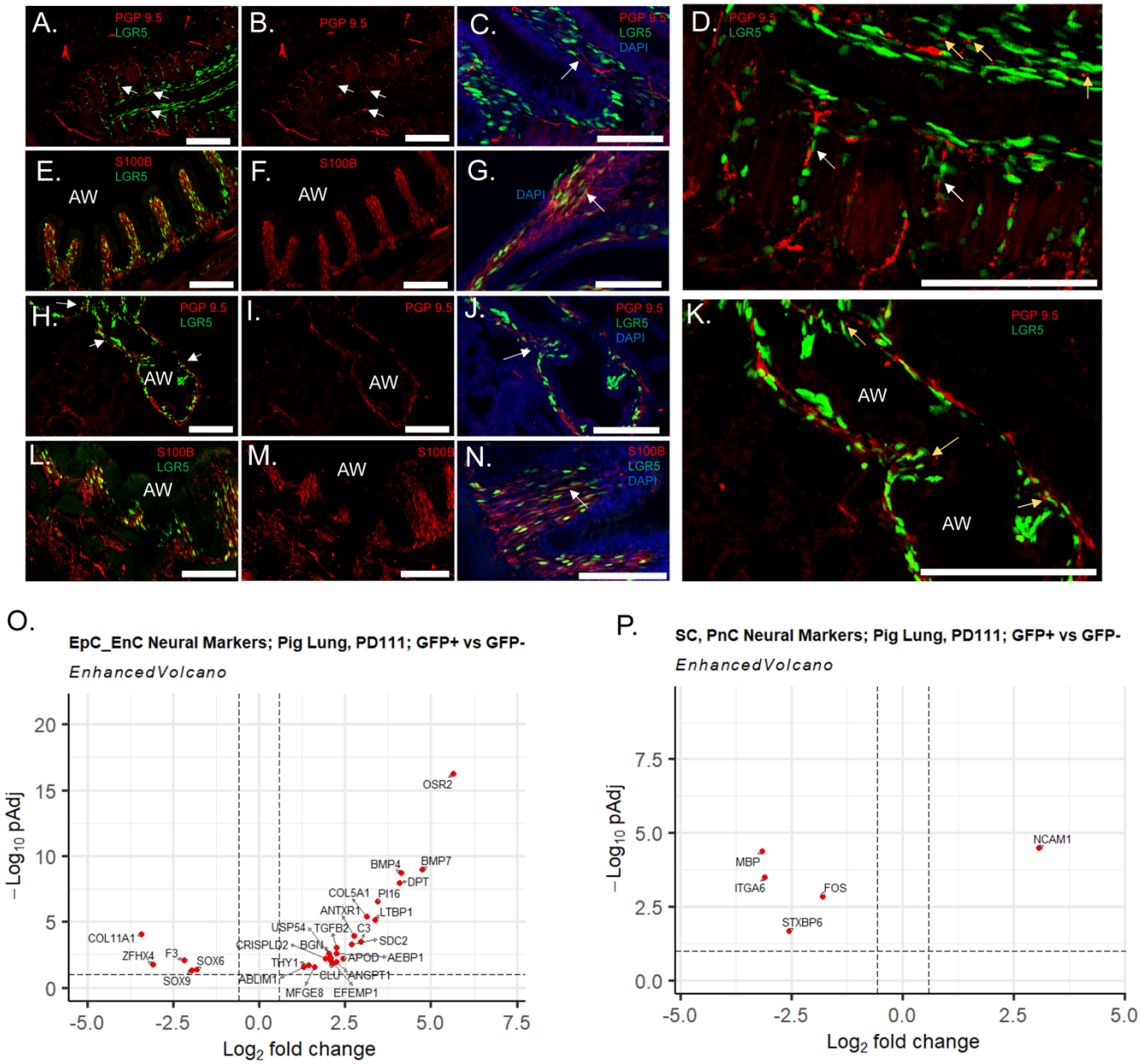

Fig 6. LGR5$^+$mesenchymal cells orient themselves along peripheral nerve fibers and express markers of nerve- associated fibroblasts. LGR5$^+$ cells identified by their intense nuclear staining orient themselves along PGP 9.5 positive fibers and express S100B at fetal GD80 (A-G) and adult PD111 (H-N). LGR5 nuclei align in an organized pattern with the longitudinal neuronal fibers of the airways. (A-B) Sagittal section showing rows of LGR5 cells running longitudinally and corresponding to the location of PGP 9.5 fibers (white arrow) (C) Crosssection of airway showing the localization of the PGP 9.5 fibers below the airway (AW) basal membrane (white arrow). (D and K) Higher magnification of a sagittal section shows that this co-localization also occurs in lateral fibers (white arrow). The punctate red staining represents cross-sections of nerve fibers, many of them in direct contact with the LGR5 cell near the nuclear region (yellow arrows). Note that while the LGR5 cells are in contact with PGP 9.5 -expressing fibers, they themselves are PGP 9.5 negative. (E-G and L-N) staining with S100B, a known Schwann cell lineage maker, showing that many, if not all fetal and postnatal LGR5 cells, also stain for S100B. (G) LGR5$^+$/S100B$^+$ cells co-localize to ganglions with concentrations of neuronal cell bodies (white arrow). (O) Volcano plot showing that genes upregulated in LGR5$^+$ mesenchymal cells are enriched for known markers of epineural and endoneurial fibroblast. (P) In contrast, few Schwann or perinuclear markers were expressed, and they were primarily downregulated.